Basis set generation for quantum dynamics simulations using simple trajectory-based methods

Maximilian A. C. Saller and Scott Habershon*

Department of Chemistry and Centre for Scientific Computing, University of Warwick, Coventry, CV4 7AL, United Kingdom

E-mail: S.Habershon@warwick.ac.uk

Abstract

Methods for solving the time-dependent Schrödinger equation generally employ either a global static basis set which is fixed at the outset, or a dynamic basis set which evolves according to classical-like or variational equations-of-motion; the former approach results in the well-known exponential-scaling with system size, while the latter can suffer from challenging numerical problems, such as singular matrices, as well as violation of energy conservation. Here, we suggest a middle road - building a basis set using trajectories to place time-independent basis functions in the regions of phase space relevant to wavefunction propagation. This simple approach, which potentially circumvents many of the problems traditionally associated with global or dynamic basis sets, is successfully demonstrated for two challenging benchmark problems in quantum dynamics, namely relaxation dynamics following photoexcitation in pyrazine, and the spin Boson model.

*To whom correspondence should be addressed

1 Introduction

Most methods for directly solving the time-dependent Schrödinger equation (TDSE[1]) introduce a linear combination of basis functions as a wavefunction *ansatz*,

$$|\psi(t)\rangle = \sum_{j=1}^{n} c_j(t)|\phi_j\rangle, \tag{1}$$

where $c_j(t)$ is a complex expansion coefficient and $|\phi_j\rangle$ is the corresponding basis function (which may comprise both nuclear and electronic degrees-of-freedom). Quantum dynamics methods employing this *ansatz* can be further sub-divided into (i) those methods which employ a time-independent basis set which is chosen at the outset,[1–4] and (ii) those methods in which the basis functions are themselves time-dependent, for example, through the temporal behaviour of a set of parameters.[5–18] In both cases, the time-evolution of the linear expansion coefficients is derived by application of the Dirac-Frenkel variational principle;[19–22] however, while the same variational approach can (and has) been applied to derive equations-of-motion for the basis function parameters,[23–25] it is more common to adopt approximate methods such as classical molecular dynamics (MD) or Ehrenfest trajectories.

These two approaches have distinct advantages and disadvantages. Using a time-independent basis set reduces the problem to solution of a system of linear equations describing the evolution of the expansion coefficients, but choosing a small basis set which can accurately represent the wavefunction at all times and across all configurational space is a major difficulty; indeed, one is usually forced to choose a global basis set which spans the entire phase-space of the problem, leading to redundancy and the well-known exponential-scaling problem associated with solution of the TDSE. This difficulty is avoided in the case of time-dependent basis functions, where the underlying potential energy surface naturally guides basis set evolution towards relevant regions of configuration-space. However, unless the basis set evolution is performed variationally, the time-dependence of the basis set can violate the conservation of energy which is implicit in the TDSE;[17] furthermore, even under varia-

tional evolution, numerical difficulties related to ill-conditioning of the evolution equations can arise, meaning that converging on the correct quantum-mechanical solution is itself a challenge.[26]

In this paper, we propose and test a"middle road" for quantum dynamics simulations: we use computationally-inexpensive trajectory simulations to sample basis functions which are subsequently employed as a time-independent basis set for solution of the TDSE. The rationale for this approach is quite clear; for any given initial wavefunction, we assume that the region of phase-space which will be sampled during wavefunction propagation can be accessed by a set of trajectories with appropriate initial conditions. By using trajectory-based simulations to place basis functions, the underlying assumption is that these trajectories will at least sample the correct regions of phase-space; this is a much less stringent demand of the trajectory-simulations than expecting them to accurately describe the evolving wavefunction across all configuration space at each given instance of time. In other words, our trajectories only have to visit those regions of configuration space which will be relevant to wavefunction propagation *at some point*; the exact time-dependence of the wavefunction is addressed separately, using the complete set of basis functions sampled by the trajectories. We note that our approach is distinct from other methods using adaptive basis sets, particularly the basis expansion leaping (BEL)[27] and matching pursuit/split-operator Fourier transform[28,29] methodologies. In both cases, the movement of basis functions through phase-space is generally driven by an optimization process in which one aims to keep the basis set describing the propagating wavefunction as small as possible; in contrast, our methodology employs physically motivated trajectory simulations to restrict basis functions to the relevant region of phase-space from the outset. As noted later, our approach does not employ coordinate grids at any level (as in MP/SOFT) and is immediately employable to systems of at least 30 degrees-of-freedom, whereas BEL has been demonstrated for just three degrees-of-freedom to date. In fact, our approach is somewhat similar in spirit to the Herman-Kluk semi-classical initial value representation (HK-SCIVR) method which has found application

in a wide variety of complex systems;[30–33] the most important differences are that the time-dependent expansion coefficients which define our wavefunction are fully coupled and obey a variational principle, in contrast to the assumptions which lead to the HK-SCIVR.[33] As a final point of comparison, we note that the methodology proposed here is distinct from previous works which employed classical trajectories to generate an environment for propagation of quantum degrees-of-freedom. For example, the classically-based separable potential (CSP) method propagates a Hartree-product-type wavefunction for a subset of quantum nuclei in an effective potential generated by the remaining classical nuclei;[9] related methods have similarly employed a trajectory-based treatment of classical nuclei, but with grid-based treatment of the quantum nuclei.[34,35] This idea of using classical trajectories to provide a time-dependent potential energy surface for quantum nuclei is certainly interesting, but is inherently distinct from the approach demonstrated here, wherein classical mechanics is used to generate a basis set prior to TDSE solution.

Our approach has a number of potential advantages. Unlike the global approach, the basis functions are only placed in regions of configuration space which are directly relevant to the problem at hand; this is a result of using trajectories which evolve under the influence of the potential energy surface. As a result, we reduce redundancy, circumvent the exponential size-scaling of the basis set and replace it with a scaling which depends instead upon the time-scale of the problem and the number of trajectories we are willing to perform. Furthermore, by adopting a time-independent (albeit trajectory-guided) basis set, we avoid both the computationally-expensive propagation of the basis functions associated with variational evolution[23–25] and the problem of energy non-conservation associated with more approximate basis function evolution.[17] Finally, anticipating future applications to modelling electronically excited state dynamics in molecular systems, our approach is consistent with the local nature of *ab initio* electronic structure calculations; in other words, *ab initio* methods may be used during the trajectory simulations, and the resulting energies, forces and electronic wavefunctions can later be used in assessing Hamiltonian matrix elements for solution of the

TDSE. Of course, we pay a price for these advantages; in particular, it is not clear *a priori* which trajectories we should use and how many basis functions we should sample in a given problem.

2 Theory

Putting these problems aside for now, let's outline the method adopted here. To demonstrate our approach, we will consider a system comprising a set of nuclear degrees-of-freedoms, labelled $\mathbf{q}$, and a set of diabatic electronic states $|\alpha\rangle$. We assume that we have an initial wavefunction at $t = 0$, $|\psi(\mathbf{q};0)\rangle|\alpha\rangle$, and our aim is to determine the wavefunction at a later time t by solution of the TDSE.

We first initiate a set of m trajectories, with initial conditions chosen to be representative of $\psi(\mathbf{q};0)$; an obvious approach might be to sample initial positions and momenta from the corresponding Wigner distribution. These trajectories, which might be classical MD trajectories, Ehrenfest trajectories or some other approximate method, are then propagated for a total of n_t time-steps during which the coordinates and momenta of each trajectory are periodically stored with a probability of $1/n_s$. Here, n_s is a user-defined factor which, along with m, controls the total size of the basis set.

The basis set used in subsequent solution of the TDSE then comprises the complete set of $N \simeq m \times (n_t/n_s)$ f-dimensional Gaussian wavepackets (GWPs) of the form

$$\langle \mathbf{q}|g_j\rangle = N_j e^{-(\mathbf{q}-\mathbf{q}_j)^{\mathrm{T}}\mathbf{A}_j(\mathbf{q}-\mathbf{q}_j)+\frac{i}{\hbar}\mathbf{p}_j\cdot(\mathbf{q}-\mathbf{q}_j)}, \tag{2}$$

where N_j is the appropriate GWP normalisation constant, $\mathbf{A}_j$ is an $f \times f$ diagonal matrix with entries $\gamma_\kappa/\hbar$, where κ labels the degree-of-freedom, and $\{\mathbf{q}_j, \mathbf{p}_j\}$ are the position and momenta of the corresponding trajectory. In other words, we use trajectories to generate a large set of GWP basis functions on a non-uniform grid; because these basis functions are sampled from trajectories originating from the phase-space spanned by $\psi(\mathbf{q};0)$, our

assumption is that they are most relevant for propagation of $\psi(\mathbf{q};0)$. Finally, we note that all calculations here use fixed-width GWPs; in other words, γ_κ is a constant for each degree-of-freedom κ.

After generating the GWP basis set, we solve the TDSE to give the time-evolution of the linear expansion coefficients in Eq. 1. Assuming that we have available a set of diabatic electronic states (as in the problems to be treated below), our *ansatz* for the total wavefunction of the system is,

$$\psi(\mathbf{q};t) = \sum_{j=1}^{n} c_j(t)|g_j\rangle|\alpha_j\rangle, \tag{3}$$

where $|\alpha_j\rangle$ labels the diabatic state for basis function j. Applying the time-dependent variational principle,[19–22] the time-dependence of the coefficients is given by,

$$\dot{\mathbf{c}} = -\frac{i}{\hbar}\mathbf{S}^{-1}\mathbf{H}\mathbf{c}, \tag{4}$$

where $\mathbf{S}$ and $\mathbf{H}$ are, respectively, the overlap and Hamiltonian matrices evaluated in the GWP basis set. The trajectory-guided approach taken in this work is schematically compared to more standard methods for solving the TDSE in Fig. 1.

The final aspect of our basis set sampling strategy relates to the positioning of GWP basis functions on the diabatic states. As in the choice of trajectories (see below), there is some flexibility here; for example, if Ehrenfest trajectories are employed in modelling a system with two electronic states, one approach might be to place GWPs on diabatic states $|1\rangle$ and $|2\rangle$ with probabilities of $|a_1|^2$ and $|a_2|^2$, respectively, where $a_{1,2}$ are the Ehrenfest expansion coefficients for each state. In this work, we chose to place a GWP on each available diabatic state at the same point in the nuclear phase-space (on average every $1/n_s$ time-steps); in other words, when storing GWPs, we simultaneously add $|g(\mathbf{q}_t,\mathbf{p}_t;t)\rangle|1\rangle$ and $|g(\mathbf{q}_t,\mathbf{p}_t;t)\rangle|2\rangle$ to the full basis set. Our initial calculations have found that this "mirrored" trajectory sampling approach gives a slightly better description of non-adiabatic dynamics

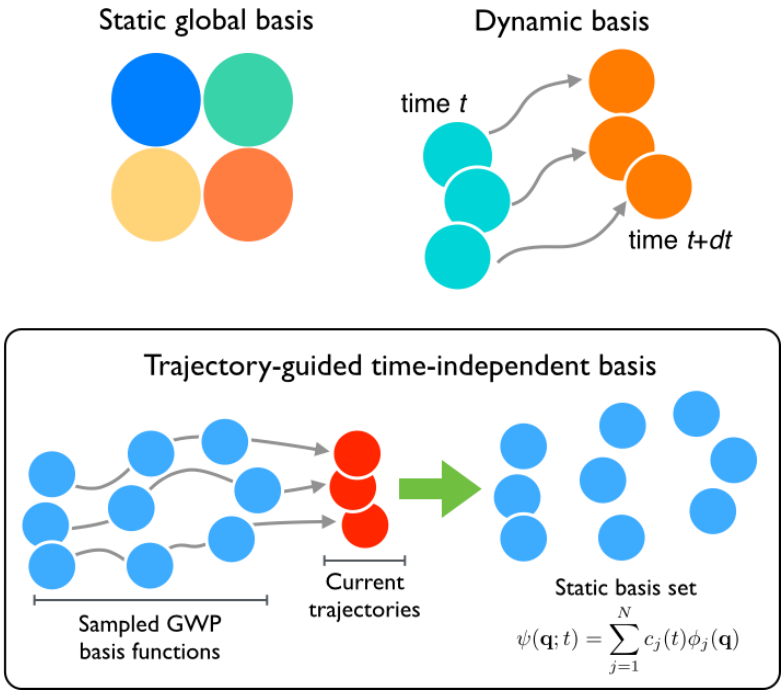

Figure 1: Overview of basis set strategies for solving the TDSE; in all cases, the wavefunction is represented as a linear combination of GWPs, the phase-space positions of which are represented by circles here. In the current work (lower panel), GWPs are positioned during computationally-inexpensive trajectory-based simulations in order to generate a non-uniform GWP basis set. The sampled GWPs are then used as a time-independent basis set for solution of the TDSE.

than a probabilistic method, probably due to the improved overlap between basis functions on different electronic states. Finally, we note that this idea of "mirrored" trajectories has been employed previously in AIMS simulations,[36] though only in the context of improving the description of non-adiabatic population transfer at short times.

3 Application, results and discussion

To demonstrate our approach, we consider non-adiabatic dynamics in two different model systems; the vibronic Hamiltonian description of pyrazine photodynamics, and the spin Boson model. Due to the availability of numerically exact simulations results,[37,38] both models have been previously employed as benchmark problems in the development of new simulations methods. Furthermore, these models are multidimensional in nature, and require

a description of dynamics on coupled electron states; as a result, they provide a stern test of any quantum simulation method. Finally, we note that our approach is trivially exact for one-dimensional problems, for which sampling trajectories with sufficiently high energy can always be used to sample the relevant phase-space of the problem.

3.1 Vibronic Hamiltonian for pyrazine

Following excitation from the ground-state S_0 to the second excited electronic state S_2 of pyrazine, the system undergoes transfer of population from S_2 to the vibronically-coupled S_1 state;[39,40] the experimentally-observed fast relaxation from S_2 to S_1 is attributed to the presence of a conical intersection, and results in a broad S_2 absorption spectrum with little discrete structure evident. To accurately describe the relaxation from S_2 to S_1, a vibronic Hamiltonian has been developed which explicitly accounts for all $f = 24$ nuclear degrees-of-freedom in the problem, as well as the two electronic excited states; it is this vibronic Hamiltonian which we consider here.[37]

In the basis of diabatic electronic states, the vibronic Hamiltonian for pyrazine can be written as[37]

$$\begin{aligned}\hat{H} = \quad & \sum_{i=1}^{f}\left[-\frac{\omega_i}{2}\frac{\partial^2}{\partial q_i^2}+\frac{\omega_i}{2}q_i^2\right]+\begin{pmatrix}-\Delta & 0\\ 0 & \Delta\end{pmatrix}+\sum_{i\in G_1}\begin{pmatrix}a_i & 0\\ 0 & b_i\end{pmatrix}q_i \\ & +\sum_{(i,j)\in G_2}\begin{pmatrix}a_{ij} & 0\\ 0 & b_{ij}\end{pmatrix}q_iq_j+\sum_{i\in G_3}\begin{pmatrix}0 & c_i\\ c_i & 0\end{pmatrix}q_i \\ & +\sum_{(i,j)\in G_4}\begin{pmatrix}0 & c_{ij}\\ c_{ij} & 0\end{pmatrix}q_iq_j,\end{aligned}$$

where q_i is the dimensionless normal-mode coordinate of the ith vibrational mode, ω_i is the associated vibrational frequency, 2Δ is the energy separation of the S_1 and S_2 states at the origin of the nuclear coordinate-space, and a_i, b_i, c_i, a_{ij}, b_{ij} and c_{ij} are a set of parameters which describe linear and bilinear expansion terms, as well as the related coupling between the states. The f vibrational modes of the problem are sub-divided into groups; G_1 is the

set of modes having A_g symmetry, G_2 is the set of pairs of modes with identical symmetry, G_3 is comprised of a single mode of B_{1g} symmetry and G_4 is the set of all pairs of modes for which the product has B_{1g} symmetry. These sub-divisions reflect the fact that a vibrational mode which couples the S_1 state (B_{3u}) and the S_2 state (B_{2u}) must be of B_{1g} symmetry. The parameters of the vibronic Hamiltonian description of pyrazine have been determined previously from a combination of experimental data and *ab initio* simulation results.[37]

As a test of our simulation approach, the full-dimensional $f = 24$-mode problem presents a formidable challenge; instead, we first consider the simpler model with $f = 4$ vibrational modes, as has also been considered by several other groups.[16,23,25,29,37,41] In this reduced-dimensional model, the vibronic coupling mode ν_{10a} and the three A_g modes with strongest linear coupling parameters, namely ν_{6a}, ν_1 and ν_{9a}, are included in the model. The initial wavefunction corresponds to a ground-state vibrational wavepacket projected onto the S_2 state,

$$\psi(\mathbf{q}; t = 0) = \left[\prod_{k=1}^{f} \left(\frac{1}{\pi}\right)^{\frac{1}{4}} e^{-\frac{1}{2}q_k^2}\right] |2\rangle \tag{5}$$

Following previous work, we focus on simulating three properties of interest. First, we calculate the autocorrelation function (or survival amplitude), $C(t)$, defined as

$$C(t) = \langle\psi(0)|e^{-i\hat{H}t/\hbar}|\psi(0)\rangle = \langle\psi(0)|\psi(t)\rangle. \tag{6}$$

Second, we calculate the S_2 photoabsorption spectrum, $I(\omega)$, which is related to the Fourier transform of $C(t)$ according to,

$$I(\omega) \propto \omega \int_{-\infty}^{+\infty} dt\, C(t) e^{-i\omega t}. \tag{7}$$

The S_2 photoabsorption spectrum of pyrazine has been measured experimentally;[39,40] however, it has been found that a phenomenological damping factor must be introduced into calculated results in order to reproduce the inherent broadening of the experimental spec-

trum.[37] Here, $C(t)$ is multiplied by an exponential function,

$$g(t) = e^{-\frac{|t|}{\tau}}, \tag{8}$$

where τ is a model-dependent damping time-constant. We note that the use of the exponential damping factor in the calculation of the absorption spectrum is not an essential feature of our methodology and is included simply for comparison to previous simulations; in fact, the exact and simulated spectra determined with g(t)=1 show a comparable level of agreement with the results presented here. Furthermore, to remove numerical artefacts in the Fourier transformation of $C(t)$ which may arise as a result of the finite simulation time for $C(t)$, we also multiply by a cosine sampling function given by

$$h(t) = \cos\left(\frac{\pi t}{2t_{\max}}\right), \tag{9}$$

where $t_{\max}$ is the maximum simulation time for $C(t)$.

The final observable of interest is the diabatic population of the S_1 state. Given the definition of our time-dependent wavefunction (Eq. 3), the population of the S_1 state is

$$P_1(t) = \sum_{i,j} c_i^* c_j \langle g_i | g_j \rangle \delta_{\lambda_i,1} \delta_{\lambda_j,1}, \tag{10}$$

where λ_j is a label indicating whether the jth GWP basis function sits on the S_1 state ($\lambda_j = 1$) or S_2 state ($\lambda_j = 2$); clearly, this definition exploits the fact that the diabatic electronic states are orthonormal. The state population $P_1(t)$ indicates the extent to which the wavepacket, initially on S_2, has transferred onto the S_1 state; as shown below, it is a sensitive indicator of whether our simulation approach is capable of treating non-adiabatic transitions correctly.

It remains to define the trajectory sampling method which was employed in the simulations of the pyrazine vibronic Hamiltonian. Given our interest in modelling systems with

multiple electronic states, we restrict ourselves to mean-field (Ehrenfest) trajectories in order to account for non-adiabatic transitions in the sampling trajectories. A similar trajectory approach has been taken in the multi-configuration Ehrenfest (MCE[16]) method; however, in that case, Ehrenfest trajectories are used to guide a basis set of *time-dependent* GWPs, rather than create a *time-independent* basis set as in this work.

Here, the initial position and momenta of each of the m sampling trajectories were sampled from the Wigner distribution of the initial wavefunction. Restricting our discussion to a system of two electronic diabatic states, each sampling trajectory represents a time-evolving wavepacket constructed as

$$|\phi(t)\rangle = \left[a_1(t)|1\rangle + a_2(t)|2\rangle\right] |g(\mathbf{q}_t, \mathbf{p}_t; t)\rangle, \tag{11}$$

where $a_{1,2}$ are expansion coefficients for the $|1\rangle$ and $|2\rangle$ diabatic states, respectively. The positions and momenta which define the GWP, $\mathbf{q}_t$ and $\mathbf{p}_t$, evolve according to mean-field equations-of-motion,

$$\frac{\partial q_\kappa}{\partial t} = \frac{p_\kappa}{m_\kappa}, \tag{12}$$

$$\frac{\partial p_\kappa}{\partial t} = -\frac{\partial V_{Ehr}}{\partial q_\kappa}, \tag{13}$$

where V_{Ehr} is a state-averaged potential energy surface given by,

$$V_{Ehr} = \frac{|a_1|^2 V_{11} + |a_2|^2 V_{22} + 2\mathrm{Re}(a_1^* a_2 V_{12})}{|a_1|^2 + |a_2|^2}, \tag{14}$$

and V_{ij} is the ij-th matrix element of the potential energy of the system. The expansion coefficients of each state, $a_{1,2}$, evolve according to the TDSE, accounting for the time-dependence of the GWP position and momenta,

$$\dot{\mathbf{a}} = -\frac{i}{\hbar}\left[\mathbf{H} - i\hbar\dot{\mathbf{S}}\right]\mathbf{a}. \tag{15}$$

Here, $\mathbf{H}$ is the Hamiltonian matrix (in the electronic basis) with elements $H_{ij} = \langle g_t|\langle i|\hat{H}|j\rangle|g_t\rangle$ and $\dot{\mathbf{S}}$ is a time-derivative matrix with elements

$$\dot{S}_{ij} = \delta_{ij}\left[\sum_{\kappa=1}^{f}\left\langle g_t\middle|\frac{\partial g_t}{\partial q_\kappa}\right\rangle\frac{\partial q_\kappa}{\partial t} + \left\langle g_t\middle|\frac{\partial g_t}{\partial p_\kappa}\right\rangle\frac{\partial p_\kappa}{\partial t}\right]. \tag{16}$$

In the simulations presented here, the positions and momenta of the GWP, and the expansion coefficients $a_{1,2}$, were evolved using an evolution scheme previously implemented for *ab initio* multiple spawning (AIMS[10–13,36,42–44]) simulations.

All calculations were performed with a time-step of 0.1 fs; sampling trajectories were run for a total of 150 fs and the TDSE was also solved for 150 fs. During each sampling trajectory, the current GWP $|g(\mathbf{q}_t, \mathbf{p}_t; t)\rangle$ at a given time-step was stored with a probability of $1/n_s$; here, we chose $n_s = 100$ and we note that the final result is reasonably insensitive to the exact value of n_s. Simulations were repeated using $m = 100$, 400 and 750 sampling trajectories, resulting in total sampled basis-set sizes of approximately 3000, 12000 and 24000 GWPs. For each system size, we performed five independent simulations; the results presented below represent averages over these five runs. In the TDSE simulations, the fourth-order Runge-Kutta integration algorithm was employed to evolve the time-dependent expansion coefficients, and initial expansion coefficients were determined by projection onto the initial wavepacket. Finally, all Hamiltonian matrix elements were calculated analytically, and the fixed widths of all degrees-of-freedom was $\gamma = 0.5$.

Figure 2 illustrates results for the autocorrelation function $C(t)$ and S_2 photoabsorption spectrum $I(\omega)$ using our trajectory-based approach. Even for the smallest of these basis sets, we find excellent agreement with the exact (grid-based[29]) $C(t)$. As the basis set size is increased, the calculated $C(t)$ converges towards the exact result such that, for the largest basis set employed, the exact and simulated results are almost indistinguishable. Notably, our simulated results are always least accurate at longer-times; this is most likely a result of the inherent "spreading-out" of the initial wavefunction throughout phase-space at longer

times, suggesting that the long-time accuracy required will have an important bearing on the necessary number of GWPs in the basis set. However, the long-time inaccuracies observed here may also arise due to the fact that we employ approximate sampling trajectories based on mean-field potential energy surfaces; as is well known, such quantum/classical trajectories are not guaranteed to possess the correct long-time behaviour, principally as a result of errors in treating zero-point energy.[45,46] Finally, Fig. 2 also shows the results for the S_2 photoabsorption spectrum, $I(\omega)$. Most strikingly, we find that even our smallest simulation gives a result which is almost indistinguishable from the exact result; this is clearly a result of the fact that $I(\omega)$ is calculated using a damped autocorrelation function and, as a result, is less sensitive to errors at long-time in $C(t)$. These results further serve to suggest that relying on comparison to exact or experimental spectra for this problem is not a particularly sensitive test of accuracy in a given simulation method.

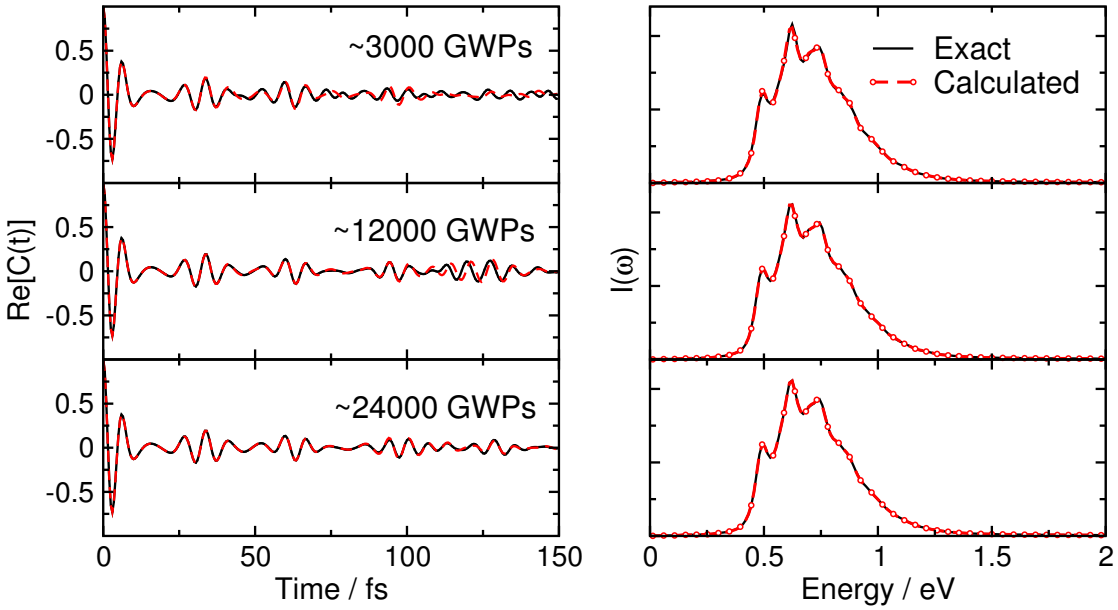

Figure 2: Calculated autocorrelation function $C(t)$ and S_2 photoabsorption spectrum $I(\omega)$ for 4-mode pyrazine vibronic Hamiltonian calculated with approximately 3000 GWPs (top row), 12000 GWPs (middle row) and 24000 GWPs (bottom row) sampled for solution of the TDSE.

Figure 3 illustrates the diabatic population of the S_1 state calculated with increasing basis set size. Again, even for the (very small) total basis set of 3000 GWPs, we observe

qualitatively accurate population dynamics; for example, the recurrence at about 80 fs is clearly observed, but we find that the long-time populations are somewhat inaccurate. As expected, the quality of the calculation increases as the basis set size increases; 12000 sampled GWPs gives excellent agreement with the overall dynamics, while 24000 GWPs further improves on this. We note here that the convergence of the population dynamics seems to be much slower than the convergence of $C(t)$ in Fig. 2; this may be a consequence of the fact that $P_1(t)$ reports on dynamics across the entire intersection of the two diabatic states, whereas $C(t)$ naturally reports on the wavefunction behaviour in the vicinity of the initial wavefunction. In any case, the results of Fig. 3 clearly demonstrate that our simulation approach is at least qualitatively correct, even for small basis sets, and can be systematically improved upon by simply running more sampling trajectories.

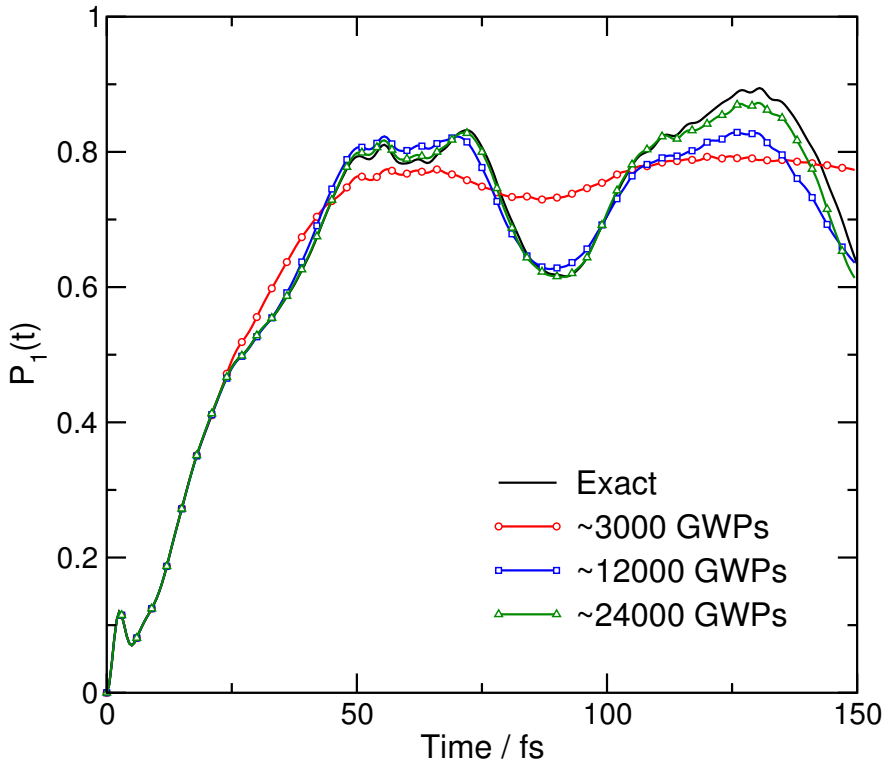

Figure 3: Time-dependent population, $P_1(t)$, of the lower diabatic state as calculated with three different basis set sizes for the 4-mode vibronic pyrazine Hamiltonian.

Finally, we consider the full-dimensional ($f = 24$) vibronic Hamiltonian for pyrazine. As noted above, this is an extremely challenging test for any quantum simulation method,

requiring accurate description of nuclear and electronic dynamics within a multidimensional space; however, this system serves as an important benchmark due to the availability of numerically-exact simulation results from the multiconfigurational time-dependent Hartree (MCTDH) method.[37] Figure 4 illustrates the calculated population transfer dynamics and autocorrelation function for our simulations employing 21000 GWPs generated in 700 Ehrenfest sampling trajectories. As expected, the agreement with MCTDH for this basis set is not perfect, although it is clear that our simple trajectory-guided approach correctly captures the qualitative population dynamics in this multidimensional system, including the population recurrence at around 80 fs. The calculated correlation function $C(t)$ is also in good agreement with the MCTDH results, although the oscillatory structure in our $C(t)$ calculations appears to be overestimated compared to MCTDH. Despite this, it is clear that our simple quantum dynamics approach reproduces the behaviour of the population dynamics in this 24-dimensional system to a sufficient level of accuracy to infer, for example, the existence of rapid population transfer from S_2 to S_1 *via* a conical intersection.

Overall, we can conclude from these simulations that our trajectory-guided approach can quickly provide qualitatively accurate results using quite small basis sets, and can be systematically improved simply by increasing the number of sampling trajectories. Furthermore, we note that we have done little to optimise our approach; alternative choices of trajectory sampling and GWP placement strategies may improve these simulations further. Finally, we note that all calculations performed here have employed full matrix storage; on going to larger basis set sizes, we can clearly exploit sparsity in the overlap and Hamiltonian matrices required for solution of the TDSE, thereby reducing computational expense.

3.2 Spin Boson model

In the second demonstration of our approach we choose another challenging problem, namely the spin Boson (SB) model.[38] The SB Hamiltonian describes a two-level electronic system linearly coupled to a bath of harmonic oscillators, and is the prototypical model of energy

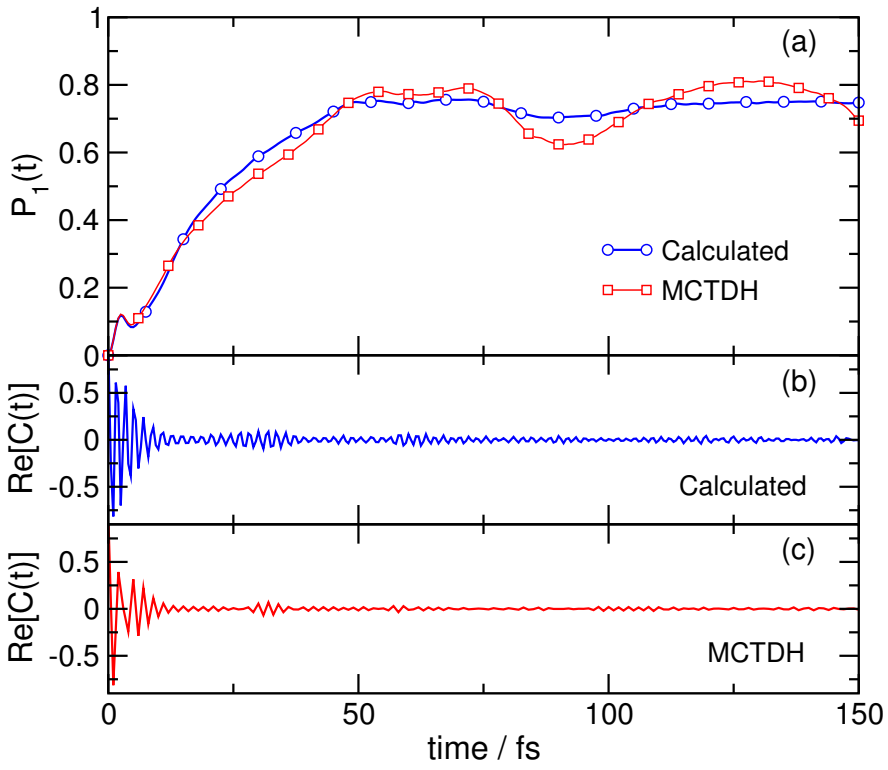

Figure 4: (a) Time-dependent population of S_1 state following photoexcitation to the S_2 state in the 24-mode pyrazine vibronic Hamiltonian; results are compared to MCTDH calculations.[37]

transfer following photoexcitation in a dissipative environment. The SB model represents a tough challenge for our methodology; for example, this many-dimensional system lies beyond the reach of the standard global basis approach of quantum dynamics unless one specifically exploits the form of the potential. The need to perform thermal ensemble-averaging introduces a further test of our trajectory-based method, which must be able to sample appropriate basis functions for a range of different initial thermal wavepackets.

The explicit Hamiltonian for the f-dimensional SB system is

$$\hat{H} = \epsilon\hat{\sigma}_z + \Delta\hat{\sigma}_x + \hat{\sigma}_z \sum_{k=1}^{f} c_k q_k + \sum_{k=1}^{f} \left[\frac{p_k^2}{2m_k} + \frac{1}{2} m_k \omega_k^2 q_k^2 \right], \tag{17}$$

where $\hat{\sigma}_x$ and $\hat{\sigma}_z$ are the usual Pauli spin matrices, ω_k is the frequency of the kth oscillator and c_k is the corresponding coupling parameter between the oscillator and the electronic

subsystem. The harmonic bath is characterised through it's spectral density, $J(\omega)$; in the present work, we use a Debye spectral density of the form

$$J(\omega) = \frac{\eta\omega_c\omega}{(\omega^2 + \omega_c^2)}, \tag{18}$$

where η is the coupling strength between the bath and the electronic sub-system, and ω_c is the cutoff frequency. The bath is dicretised into $f = 30$ modes with the bath frequencies ω_k and coupling strengths c_k given by,

$$\omega_k = \omega_c \tan\left(\frac{\pi}{2f}\left[k - \frac{1}{2}\right]\right), \tag{19}$$

$$c_k = \omega_k\sqrt{\frac{\eta}{f}}. \tag{20}$$

This discretisation scheme ensures that the exact electronic reorganisation energy is obtained.[18,47–49] Finally, all degrees-of-freedom have mass $m_k = 1$, we employ atomic units such that $\hbar = k_B = 1$, and units are given relative to the inter-state coupling value Δ.

The time-dependent property of interest is the thermally-averaged population difference between the two excited states, given by

$$P(t) = \frac{1}{Z_B}\mathrm{Tr}\left[e^{-\beta\hat{H}_b}|1\rangle\langle 1|e^{+i\hat{H}t/\hbar}\hat{\sigma}_z e^{-i\hat{H}t/\hbar}\right]. \tag{21}$$

Here, the initial Boltzmann density operator is chosen such that the system is prepared in an equilibrium state for the bath degrees-of-freedom (so $\hat{H}_b$ corresponds to the final summation of Eq. 17) and the system then undergoes a Franck-Condon transition to the excited state $|1\rangle$. Inserting complete sets of coordinate eigenstates allows one to write $P(t)$ as

$$P(t) = \frac{1}{Z_B}\int d\mathbf{q}\, d\mathbf{q}_1 \left[P_1(\mathbf{q};t) - P_2(\mathbf{q};t)\right], \tag{22}$$

where

$$P_k(\mathbf{q};t) = \frac{|\langle k\mathbf{q}|e^{-\beta\hat{H}_B/2-i\hat{H}t/\hbar}|\mathbf{q}_1 1\rangle|^2}{Z_B}. \tag{23}$$

As shown in recent work,[18] the initial population function $P_1(t=0)$ may be generated quite straightforwardly in a path-integral molecular dynamics (PIMD) simulation. In particular, $P_1(t=0)$ is proportional to the density of points at imaginary-time values of $\beta/2$ following propagation from a fixed point q_1; by assuming a Gaussian density distribution, as is common in approaches such as the variational Gaussian method of Mandelshtam and coworkers,[50–53] $P_1(t=0)$ may be easily calculated in a constrained equilibrium path-integral calculation. Because the real-time evolution of $P_1(t=0)$ obeys the TDSE, the trajectory-based simulation method proposed here may be used to propagate this initial thermal wavepacket; Eq. 22 indicates that averaging $P(t)$ over many such initial wavepackets allows one to calculate the thermally-averaged time-dependent population difference.

In the calculations illustrated here, we considered three different sets of SB model parameters for which numerically-exact simulation results are available.[38] In set (a), corresponding to the intermediate ($\omega_c/\Delta \simeq 1$) bath regime, we chose $\omega_c = 1.0$, $\eta = 5.0$, $\beta = 1.0$ and $\epsilon = 0.0$. In set (b), we chose $\omega_c = 0.25$, $\eta = 5.0$, $\beta = 5.0$ and $\epsilon = 0.0$, corresponding to the adiabatic bath regime ($\omega_c/\Delta < 1$). Finally, in set (c), we chose $\omega_c = 5.0$, $\eta = 0.5$, $\beta = 0.5$ and $\epsilon = 1.0$, giving an example of a SB model with a non-zero bias between the energies of the diabatic electronic states. For these simulations, the initial thermal wavepacket was generated in a constrained PIMD simulation using 250 ring-polymer beads (or Trotter slices), 8 - 12 GWP sampling trajectories were initiated for each thermal GWP, and propagation results for 1000 initial thermal GWPs were averaged to give the final thermal population functions. In all calculations, the widths of the sampled GWPs were set to be identical to the widths of the initial thermal wavepacket as sampled by path-integral sampling.[18]

To demonstrate that our approach is flexible with regards to the sampling trajectories employed, we used simple classical trajectories initiated on the $|1\rangle$ and $|2\rangle$ diabatic states alternately in order to generate a GWP basis set for propagation of each initial thermal

wavepacket. In total, our calculations employed a basis set of between 1800 and 2400 GWPs for each initial thermal wavepacket. Following our previous work,[18] we note that, because our sampling strategy for generating initial thermal wavepackets only yields the *density*, the choice of initial momenta for the GWP sampling trajectories is somewhat arbitrary. In this work, we chose to sample from the classical Boltzmann distribution in the case of (b) and (c), and from the Wigner distribution in the case of (a). Finally, for comparison, we calculated the time-dependent populations using the Ehrenfest (mean-field) approach with initial bath conditions sampled from the Wigner distribution and final populations averaged over 2000 trajectories.[54]

Figure 5 shows the results of our trajectory-guided simulations for the SB model. As expected based on our experiences with the pyrazine model, we find that our simple simulation strategy, combined with path-integral sampling of initial thermal GWPs, can capture the qualitatively correct quantum dynamics in each case. The agreement with the exact results in the intermediate regime (Fig. 5(a)) is surprisingly good, and clearly better than the standard Ehrenfest approach. Similarly, in the adiabatic bath regime (Fig. 5(b)), our simulations clearly capture the oscillations in the diabatic state populations and the long-time limit is in much better agreement with the exact result than the Ehrenfest result is. Finally, we find that our simple approach can reproduce the qualitative population dynamics in the asymmetric SB model (Fig. 5(c)); the agreement with the exact result here is much better than the Ehrenfest result, but is clearly not as good as in the two other cases considered. The most likely explanation for this is our dependence on classical trajectories to place basis functions. It is well known that methods based upon classical trajectories can fail to correctly describe long-time dynamics in non-zero-bias SB models as a result of errors in the treatment of ZPE;[45,46,54] as a result, it seems likely that the long-time accuracy of our trajectory-based approach may suffer because basis functions are increasingly placed in regions of phase-space which are not consistent with the exact quantum dynamics of the system. However, we note that, unlike the Ehrenfest method and similar approaches where classical trajectories are

used to directly construct quantum information, our approach can be made increasingly accurate by simply increasing the number of sampled GWPs. A more efficient alternative is clearly to choose trajectory-generation methods which result in more accurate sampling of the relevant phase-space at longer-times; one example might be RPMD,[55,56] which yields the exact quantum Boltzmann distribution,[57] although this is clearly an avenue for further work.

Overall, we find that the performance of our trajectory-guided simulation approach is better that the established Ehrenfest method, and performs comparably to other methods which are specifically adapted to work for system-bath models.[54] This level of performance is particularly encouraging, given that we have done little to optimise our approach.

Computational effort. As a final point, it is worth considering how our approach fares in terms of computational expense. Running m trajectories of length n_t time-steps, followed by solution of the TDSE for n_t time-steps, will require a total computational time of approximately

$$t = amn_t + b\left(\frac{mn_t}{n_s}\right)^3 + cn_t\left(\frac{mn_t}{n_s}\right)^2 \tag{24}$$

where a, b and c are characteristic constants representing the time for performing one time-step of a trajectory, calculating Hamiltonian, overlap and inverse overlap matrices, and propagation of the complex expansion coefficients by continued matrix-vector multiplication, respectively (Note that we have assumed the worst-case scenario for matrix manipulations). Note that the overall effort of the approach does not explicitly depend on the number of degrees-of-freedom in the system; the system dependence is instead reflected in the number of GWPs which will be required to obtain converged results. In many applications, generating classical (or related) trajectories is relatively inexpensive from the computational viewpoint; instead, the computational expense of our approach is dominated by construction of the Hamiltonian, overlap and inverse overlap matrices, as well as propagation by large-scale matrix-vector multiplications. However, there is much scope to improve all of these

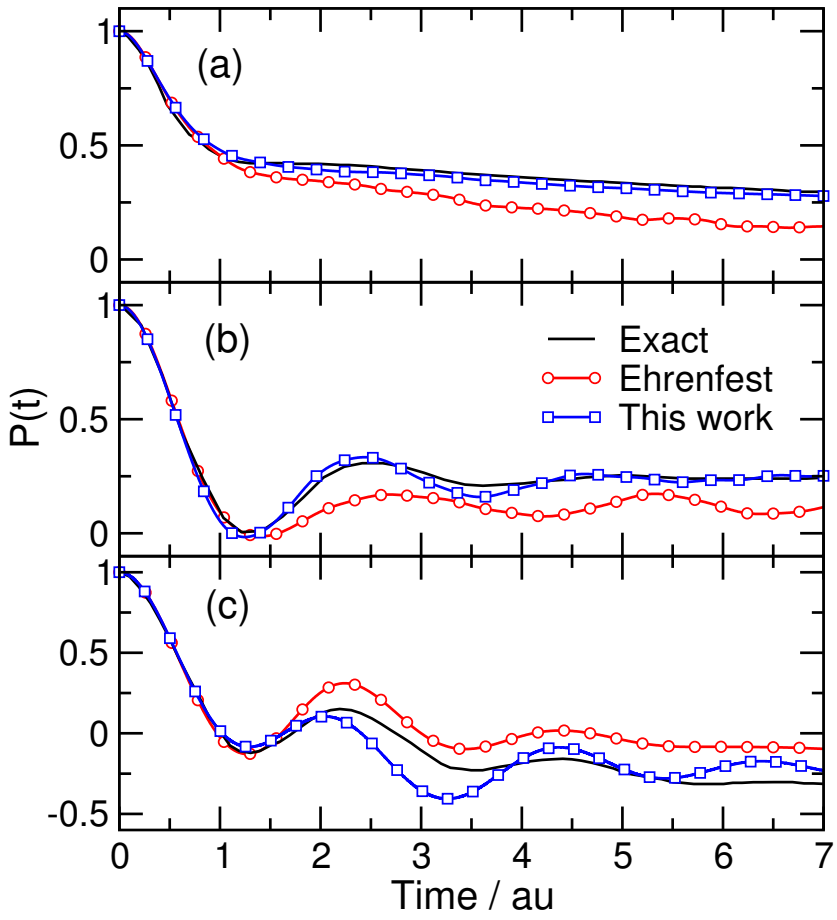

Figure 5: Population difference functions $P(t)$ calculated in trajectory-guided quantum simulations of the SB model with parameters chosen to give (a) the intermediate bath regime, (b) the adiabatic bath regime, and (c) a non-zero energetic bias between the electronic states. In each panel, results are shown for numerically exact simulations,[38] Ehrenfest method and our trajectory-guided approach.

bottle-necks; for example, the Hamiltonian and overlap matrices will generally be sparse, particularly in higher-dimensional problems, allowing efficient sparse matrix methodologies to be employed. Furthermore, there is scope to employ potential energy information generated during the course of sampling trajectories in the evaluation of Hamiltonian matrix elements, as in the "Grow" method.[58] Each of these features will make large savings in the computational time of our simulations, and are currently being explored.

4 Conclusions

In this article, we have demonstrated a very simple approach to modelling (non-adiabatic) quantum dynamics in many-dimensional systems using trajectory-guided basis sets. Our results show that, using simple Ehrenfest or classical MD trajectories, the basis sets produced are compact and suitable for solution of the TDSE. An important advantage (or, perhaps, disadvantage) of this approach is it's flexibility; we are free to generate the basis set using any trajectory-based method we see fit, and the size of the basis set is also under our control. In the future, we will investigate the use of surface hopping[59] and AIMS[10–13,36,42–44] trajectories as the next level of approximation, although we could also consider using variational GWP trajectories. Finally, we note that both problems considered here are somewhat simplified by having a known set of diabatic states available; current work is aimed at combining our trajectory-based approach with *ab initio* electronic structure calculations for the potential energy surfaces and their couplings. Taking into account the efficiency of our trajectory-based method, this overall methodology should prove useful in modelling quantum chemical dynamics in a variety of systems, particularly photochemical reactions in solvent environments, where there is often a clear distinction between the quantum system and an environment which can be treated classically.

While straightforward application of our approach has been shown to reproduce qualitative quantum dynamics in many-dimensional problems, there are some clear avenues which could be explored to improve our methodology. First, there is nothing in our current approach to prevent regions of phase-space being either under- or over-sampled by basis functions. While sparse sampling can, in principle, be addressed by increasing the number of sampling trajectories, this may be inefficient. Instead, we are currently exploring methods whereby further GWP basis functions can be generated to "fill in" sparsely-sampled regions of phase-space without performing further trajectory simulations; one obvious approach is to exploit the fact that sampled GWPs can be used in a configuration interaction-type framework, whereby orbitals from two different sampled GWPs are swapped to generate new

intermediate GWPs. These methods will increase the total size of the basis set but, as noted above, will also benefit from employing sparse matrix methods. In contrast, over-sampling in regions of phase-space may lead to linear dependence in the basis set; at the moment, we are currently seeking to address this challenge by implementing a recently-proposed projection method for dealing with linear dependence in GWP basis sets.[17] Second, it is clear that the time-scale over which classical-like trajectories can be used to effectively sample the relevant regions of phase-space for wavefunction propagation will be somewhat problem-dependent; for example, in systems possessing strongly coupled vibrational degrees-of-freedom, non-physical flow of ZPE[57] in classical trajectories might mean that sampling basis functions at longer times becomes more difficult. We are currently exploring the possibility of using shorter time segments for trajectory-sampling, between which new sampling trajectories are initiated from the current wavefunction; while this methodology is more akin to the BEL approach,[27] an important difference is that our basis-set sampling approach is based on computationally-inexpensive yet physically-appropriate trajectories. Overall, these developments have the potential to make an important to the performance of our approach, both in terms of computational expense and accuracy.

Acknowledgement

This research was supported by start-up funding from the University of Warwick (SH), and the award of an EPSRC studentship (MACS). Computational resources were provided by the Centre for Scientific Computing at the University of Warwick.

References

(1) Tannor, D. J. *Introduction to quantum mechanics: A time-dependent perspective*; University Science Books: Sausalito, CA, USA, 2007.

(2) Park, T. J.; Light, J. C. *J. Chem. Phys.* **1986**, *85*, 5870.

(3) Sielk, J.; von Horsten, H. F.; Kruger, F.; Schneider, R.; Hartke, B. *Phys. Chem. Chem. Phys.* **2009**, *3*, 463–475.

(4) Schmidt, P. P. *Int. J. Quantum Chem.* **2002**, *90*, 202.

(5) Meyer, H.-D., Gatti, F., Worth, G. A., Eds. *Multidimensional quantum dynamics: MCTDH theory and applications*; Wiley: Weinheim, Germany, 2009.

(6) Meyer, H.-D.; Manthe, U.; Cederbaum, L. *Chem. Phys. Letters* **1990**, *165*, 73 – 78.

(7) Gerber, R. B.; Buch, V.; Ratner, M. A. *J. Chem. Phys.* **1982**, *77*, 3022.

(8) Heller, E. J. *J. Chem. Phys.* **1981**, *75*, 2923.

(9) Jungwirth, P.; Gerber, R. *J. Chem. Phys.* **1995**, *102*, 6046.

(10) Martinez, T. J.; Ben-Nun, M.; Levine, R. D. *J. Phys. Chem.* **1996**, *100*, 7884.

(11) Martinez, T. J.; Ben-Nun, M.; Ashkenazi, G. *J. Chem. Phys.* **1996**, *104*, 2847.

(12) MartÌnez, T. J. *Chem. Phys. Letters* **1997**, *272*, 139.

(13) Martinez, T. J.; Levine, R. D. *J. Chem. Soc., Faraday Trans.* **1997**, *93*, 941.

(14) Ben-Nun, M.; Martinez, T. J. *Adv. Chem. Phys.* **2002**, *121*, 439.

(15) Sherratt, P. A.; Shalashillin, D. V.; Child, M. S. *Chem. Phys.* **2006**, *322*, 127.

(16) Shalashilin, D. V. *J. Chem. Phys.* **2010**, *132*, 244111.

(17) Habershon, S. *J. Chem. Phys.* **2012**, *136*, 014109.

(18) Habershon, S. *J. Chem. Phys.* **2013**, *139*, 104107.

(19) Broeckhove, J.; Lathouwers, L.; Kesteloot, E.; Van Leuven, P. *Chem. Phys. Letters* **1988**, *149*, 547–550.

(20) Dirac, P. A. M. *Proc. Cambridge Phil. Soc.* **1930**, *26*, 376.

(21) Frenkel, J. *Wave Mechanics*; Oxford University Press: Oxford, 1934.

(22) McLachlan, A. D. *Mol. Phys.* **1964**, *8*, 39.

(23) Burghardt, I.; Giri, K.; Worth, G. A. *J. Chem. Phys.* **2008**, *129*, 174104.

(24) Worth, G. A.; Burghardt, I. *Chem. Phys. Letters* **2003**, *368*, 502.

(25) Worth, G. A.; Robb, M. A.; Lasorne, B. *Mol. Phys.* **2008**, *106*, 2077.

(26) Mendive-Tapia, D.; Lasorne, B.; Worth, G. A.; Robb, M. A.; Bearpark, M. J. *J. Chem. Phys.* **2012**, *137*, 22A548.

(27) Koch, W.; Frankcombe, T. J. *Phys. Rev. Lett.* **2013**, *110*, 263202.

(28) Wu, Y.; Batista, V. S. *J. Chem. Phys.* **2003**, *118*, 6720–6724.

(29) Chen, X.; Batista, V. S. *J. Chem. Phys.* **2006**, *125*, 124313.

(30) Herman, M. F.; Kluk, E. *Chem. Phys.* **1984**, *91*, 27 – 34.

(31) Kay, K. G. *J. Chem. Phys.* **1994**, *100*, 4377.

(32) Miller, W. H. *J. Phys. Chem. A* **2001**, *105*, 2942–2955.

(33) Miller, W. H. *J. Phys. Chem. B* **2002**, *106*, 8132.

(34) Iyengar, S. S.; Sumner, I.; Jakowski, J. *J. Phys. Chem. B* **2008**, *112*, 7601–7613.

(35) Li, X.; Oomens, J.; Eyler, J. R.; Moore, D. T.; Iyengar, S. S. *J Chem Phys* **2010**, *132*, 244301.

(36) Ben-Nun, M.; Martinez, T. J. *Isr. J. Chem.* **2007**, *47*, 75 – 88.

(37) Raab, A.; Worth, G. A.; Meyer, H.-D.; Cederbaum, L. S. *J. Chem. Phys.* **1999**, *110*, 936 – 946.

(38) Thoss, M.; Wang, H.; Miller, W. H. *J. Chem. Phys.* **2001**, *115*, 2991–3005.

(39) Yamazaki, I.; Murao, T.; Yamanaka, T.; Yoshihara, K. *Faraday Discuss. Chem. Soc.* **1983**, *75*, 395 – 405.

(40) Innes, K. K.; Ross, I. G.; Moomaw, W. R. *J. Mol. Spectrosc.* **1988**, *132*, 492 – 544.

(41) Puzari, P.; Sarkar, B.; Adhikari, S. *J. Chem. Phys.* **2006**, *125*, 194316.

(42) Ben-Nun, M.; Martínez, T. J. *J. Chem. Phys.* **1998**, *108*, 7244.

(43) Ben-Nun, M.; Quenneville, J.; Martínez, T. J. *J. Phys. Chem. A* **2000**, *104*, 5161.

(44) Ben-Nun, M.; Martinez, T. J. *J. Chem. Phys.* **2000**, *112*, 6113.

(45) Müller, U.; Stock, G. *J. Chem. Phys.* **1999**, *111*, 77 – 88.

(46) Golosov, A. A.; Reichman, D. R. *J. Chem. Phys.* **2001**, *114*, 1065 – 1074.

(47) Craig, I. R.; Manolopoulos, D. E. *J. Chem. Phys.* **2005**, *122*, 084106.

(48) Markland, T. E. Two different approaches to electronically non-adiabatic dynamics. M.Sc. thesis, Oxford University, 2006.

(49) Wang, H.; Thoss, M.; Miller, W. H. *J. Chem. Phys.* **2001**, *115*, 2979–2990.

(50) Brown, S. E.; Georgescu, I.; Mandelshtam, V. A. *J. Chem. Phys.* **2013**, *138*, 044317.

(51) Georgescu, I.; Deckman, J.; Fredrickson, L. J.; Mandelshtam, V. A. *J. Chem. Phys.* **2011**, *134*, 174109.

(52) Frantsuzov, P. A.; Mandelshtam, V. A. *J. Chem. Phys.* **2008**, *128*, 094304.

(53) Frantsuzov, P. A.; Mandelshtam, V. A. *J. Chem. Phys.* **2004**, *121*, 9247–9256.

(54) Berkelbach, T. C.; Reichman, D. R.; Markland, T. E. *J. Chem. Phys.* **2012**, *136*, 034113.

(55) Habershon, S.; Manolopoulos, D. E.; Markland, T. E.; Miller, T. F. *Annu. Rev. Phys. Chem.* **2013**, *64*, 387–413.

(56) Craig, I. R.; Manolopoulos, D. E. *J. Chem. Phys.* **2004**, *121*, 3368–3373.

(57) Habershon, S.; Manolopoulos, D. E. *J. Chem. Phys.* **2009**, *131*, 244518.

(58) Frankcombe, T. J.; Collins, M. A.; Worth, G. A. *Chem. Phys. Letters* **2010**, *489*, 242–247.

(59) Tully, J. C. *J. Chem. Phys.* **1990**, *93*, 1061–1071.

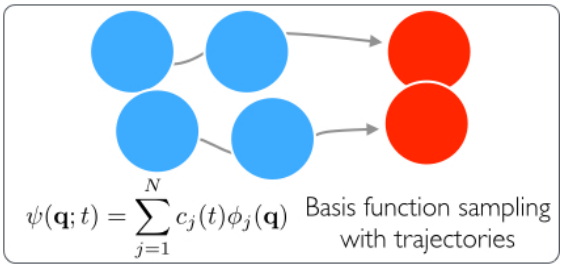

Figure 6: TOC graphic